Journal of Materials Chemistry

Cite this: J. Mater. Chem., 2011, 21, 10085

www.rsc.org/materials

PAPER

Direct synthesis of nanocrystalline $Li_{0.90}FePO_4$: observation of phase segregation of anti-site defects on delithiation

Shri-Prakash Badi,[a] Marnix Wagemaker,*[b] Brian L. Ellis,[a] Deepak P. Singh,[b] Wouter J. H. Borghols,[b] Wang Hay Kan,[a] D. H. Ryan,[c] Fokko M. Mulder[b] and Linda F. Nazar*[a]

Received 14th December 2010, Accepted 8th March 2011
DOI: 10.1039/c0jm04378h

Solid solutions of Li_xFePO_4 are of tremendous interest because of a proposed increase in ion transport properties, but the formation of these solutions at high temperatures is difficult if not impossible and direct synthesis is difficult and rarely reported. Here we report modified polyol syntheses which produce nanocrystalline $Li_{1-y}FePO_4$ directly, where the maximum Li substoichiometry on the M1 site sustained at synthesis temperatures of 320 °C is about 10%. High target lithium vacancy concentrations promote the increase in anti-site disorder of Li^+ and Fe^{2+}, as this process is driven by vacancy stabilization. Combined neutron and X-ray diffraction on partial delithiated substoichiometric olivines reveals segregated defect-free (where Li is extracted) and defect-ridden (where Li remains) regions. This proves (1) that the anti-site defects obstruct Li^+ diffusion explaining the detrimental electrochemistry and (2) that the anti-site defects form clusters. Finally, preferential anisotropic strain broadening in the *bc*-plane indicates the existence of a coherent interface between the Li-poor and Li-rich phases. Along with the size broadening upon delithiation this proves that in nano-sized Li_xFePO_4 the two phases coexist within a single particle, which is not expected based on thermodynamics arguments due to the energy penalty associated with the coherent interface. Thereby, these results give important and unique insight and understanding in the properties of nano sized $LiFePO_4$.

Introduction

Rechargeable lithium ion batteries power most portable electronic devices, with $LiMO_2$ (M = Co, Mn, Ni, Al or mixtures thereof) dominating as the cathode material of choice. Recently, olivine-type $LiMPO_4$ cathode materials have also risen to prominence. Since the initial report over a decade ago,[1,2] the iron-based olivine $LiFePO_4$ has emerged as a strong contender for high power applications such as plug-in electric vehicles (PHEVs), owing to its non-toxic nature and outstanding safety characteristics. It exhibits highly reversible cycling at 3.4–3.5 V and has a theoretical capacity of 170 mAh/g, based on a well-established two-phase redox reaction between $LiFePO_4$ and $FePO_4$. Several factors govern the rate performance of $LiFePO_4$ cells: intrinsic and surface electronic/ionic conductivity, particle size, phase transition kinetics have all been studied. Various synthesis and processing approaches have been employed to optimize the properties of $LiFePO_4$. The most common approach is coating the particle surfaces with carbon which serves to both increase the surface electronic conductivity and reduce the particle size of the active $LiFePO_4$ particles.[3–6] A more recent approach involved the use of a lithium ion conductive phosphate coating to enhance surface ionic conductivity.[7]

The extent of intrinsic electronic and ionic conductivity of $LiFePO_4$ has been greatly debated over the past decade. Chiang *et al.* reported that the electronic conductivity could be raised by 8 orders of magnitude by supervalent-cation doping, which was proposed to stabilize minority Fe^{3+} hole carriers in the lattice by stabilizing the solid solution. The dramatic increase in conductivity was later shown to instead be the result of carbon and metallic iron phosphides/carbophosphides on the $LiFePO_4$ surface arising from solid-state reactivity at the elevated temperatures used in processing.[8] The dopants are reported to exsolve from the lattice at these temperatures.[9] Although low levels of dopants can be incorporated into olivine at intermediate (ie ~600 °C) temperatures, this does not result in Li_xFePO_4 solid solutions containing Fe^{3+}. Combined neutron and X-ray diffraction of aliovalent cation compensated triphylite ($Li_{1-xy}D_x^{y+}FePO_4$, D = Zr, Nb, Cr) demonstrated that supervalent-cation doping up to ~3–4% atomic substitution can be hosted in the $LiFePO_4$ lattice in bulk materials prepared by a solid state route at 600 °C.[10] The aliovalent dopant charge is balanced by lithium vacancies, with the total charge on the iron site being +2, within the limit of experimental error. Similar

[a]Department of Chemistry, University of Waterloo, 200 University Ave. West, Waterloo, Ontario, Canada N2L 3G1
[b]Department of Radiation, Radionuclides and Reactors, Faculty of Applied Sciences, Mekelweg 15, 2629 JB Delft, The Netherlands
[c]Department of Physics, McGill University, 845 Sherbrooke St. West, Montreal, Quebec, Canada H3A 2T5

Li-site doping was carried out in lithium nickel and magnesium olivines, in which the charge of the nickel also remains +2.[11,12] The results clearly showed that the dopant resides primarily on the M1 (Li) site and is vacancy compensated, as also confirmed by later studies.[13]

The olivine structure is built up of $[PO_4]^{3-}$ tetrahedra, with the divalent M ions occupying corner-shared octahedral "M2" sites, and the Li ions occupying the "M1" sites to form chains of edge-sharing octahedra. Fast 1D conduction along the *b*-axis in the *Pnma* structure was predicted by atomistic modeling and corroborated by spectroscopic studies.[14–17] The presence of M2 site ions or dopant ions on the M1 site has been theorized to hinder ion transport along the *b*-axis, and require 3D diffusion of Li^+. Calculations show that Li–Fe mixing leads to "anti-site (Li^+:Fe^{2+}) pairs" which are the most favorable defects that can occur in olivine, and have the lowest formation energy.[18] The degree of anti-site mixing appears to be temperature dependent; defect formation at low temperature where nucleation and growth can lead to non-thermodynamically favored materials is not surprising. Anti-site mixing occurs in these olivines when they are synthesized at low temperature: hydrothermal synthesis at temperatures <130 °C produced material where 7–8 mol% Fe is located on the lithium sites.[19,20] A HAADF-STEM study has suggested that concentrations of anti-site defects as high as 1% are sustained in samples synthesized by solid state reaction at temperatures as high as 600 °C, but by 800 °C the anti-site mixing is not detectable.[21]

Nonetheless, solid solutions can be prepared at lower temperatures where thermodynamics do not govern phase stability. It has been established, for example, that Fe^{3+} hole carriers can be formed by chemical delithiation of $LiFePO_4$ at room temperature.[22] This is due to the coexistence of limited solid solution regimes defined by $Li_{1-\beta}FePO_4$ at the lithium-rich end member, and $Li_\alpha FePO_4$ at the lithium poor, where $(1-\beta) = 0.89$, and $\alpha = 0.05$ in the two phase mixtures. The extent of the solid solution regime is dependent on crystallite size. More extensive regimes are observed for smaller crystallites approaching 40 nm; and delithiation of such nanoparticles has been reported to yield a singular solid solution, $Li_{0.93}FePO_4$.[23] However, only one report exists of direct synthesis of solid solution Li_xFePO_4. Gibot *et al.* recently adopted a fine-tuned aqueous precipitation method that gives rise to nanoparticles of $LiFePO_4$ with substantial Li-substoichiometry (up to 20%) associated with the presence of Fe^{3+} and considerable Li–Fe mixing.[24] Such a nanomaterial with considerable disorder exhibits single-phase room temperature insertion, in contrast to the well-established two-phase room-temperature insertion process in $LiFePO_4$ electrodes.

Motivated by transport constraints, the drive towards reducing crystallite size has resulted in an intense examination of the effect that constrained dimensions have on defects and disorder; and on other size-dependent properties. In this paper, we report on the detailed structure of substoichiometric nanosized Li_xFePO_4 prepared by direct synthesis using the polyol method, which represents a low-intermediate temperature synthesis that can produce nanoparticles with high crystallinity.[25] We address the complex relationship of nanocrystallite-driven properties, the formation of metastable substoichiometric Li_xFePO_4 phases and anti-site defects in olivines. Combined analysis of X-ray and neutron diffraction data allows us to quantify the site disorder. Furthermore, we show that partial delithiation occurs primarily in regions without site disorder, hence domains are formed with site disorder that remain as the Li-rich phase, Li_xFePO_4, and domains without that are delithiated to form the Li-poor phase, $FePO_4$. The presence of defects in the lattice is a key aspect in the rates of intercalation and deintercalation reactions in $LiFePO_4$.

Experimental

Synthesis

$Li_{1-x}FePO_4$ ($x = 0$, 0.1, 0.2) nanoparticles with different substoichiometries were prepared *via* a modified polyol process, first reported by Kim *et al.*[25] Iron acetate (99.995%, Aldrich), ammonium dihydrogen phosphate (99+%, BDH), and lithium acetate (99.99%, Aldrich) were added to tetraethylene glycol (TEG) in ratios dictated by the target stoichiometry. The total concentration of iron in the solution was 0.25 M. The solution was refluxed at 320 °C for 3–20 h. To remove organic residues the product was washed several times with acetone and ethanol. The resulting particles were filtered and dried in a vacuum oven at 150 °C for 24 h. Phase purity of the samples was confirmed by XRD.

TEM

TEM was performed using the FEI TITAN 80–300 HB Cubed to study the morphology and size of the particles. Images were recorded at 300 kV in bright field mode.

Electrochemistry

To prepare the composite electrodes, the iron phosphate compounds were thoroughly mixed with Super S carbon and poly(tetrafluoroethylene) (PTFE) binder in a 70 : 20 : 10 wt ratio with isopropanol as the solvent. A thin sheet of this homogeneous mixture was pressed against C-coated Al foil. The electrodes were tested against lithium in coin cells, with 1 M $LiPF_6$ in EC/DMC (1 : 1 v/v) electrolyte. Cells were galvonostatically cycled (C/20 rate) using a VMP3 (Biologic, Claix, France) between 2.0 and 4.4 V.

Chemical delithiation

The prepared Li_xFePO_4 compounds were chemically delithiated to varying degrees with stoichiometric amounts of $NOBF_4$ in acetonitrile, for 30 min.

Mössbauer

Mössbauer spectra were collected using a 50 mCi ^{57}Co Rh source mounted on a constant-acceleration spectrometer, calibrated with Fe foil at room temperature. Spectra were fitted to a sum of Lorentzian lines using a conventional nonlinear least-squares minimization routine.

Diffraction and refinement

Neutron diffraction (ND) was performed on POLARIS, the time-of-flight (TOF) neutron diffraction instrument at ISIS (Rutherford Appleton Laboratories, Didcot, UK), and these data were co-refined with X-ray diffraction (XRD) data collected

on an X-pert Pro multi-phase detector, (Philips/Panalytical) using X-ray radiation from a Cu-anode (0.4×12 mm^2 line focus, 45 kV, 40 mA). To avoid air exposure, diffraction data were collected on samples in sealed holders under an Ar atmosphere.

During the fitting of the diffraction data, two neutron banks (under 90° and 145° with respect to the incident beam) were simultaneously fitted with the X-ray data; each bank was equally weighted. For neutron TOF diffraction the incident wavelength is less well defined than the X-ray data, thus the simultaneous fit was restricted to the lattice parameters from fitting the X-ray data. This was achieved by allowing the neutron diffractometer constants to vary (effectively the exact sample position in the neutron flight path). To correct for an error in the vertical alignment, a diffractometer constant zero term was fitted. The natural abundance of ^{6}Li necessitated the neutron data be corrected for a wavelength dependent absorption correction, commonly used for TOF neutron diffraction. For the three target compositions: $Li_{0.8}FePO_4$, $Li_{0.9}FePO_4$, and $Li_{1.0}FePO_4$, 30 wt % Si powder was mixed as an internal reference to accurately determine the lattice parameter.

Both Fe and Li were allowed to occupy both the M1 (Li) sites and the M2 (Fe) sites to account for possible site disorder. The amount of Li on the M2 site and Fe on the M1 site were coupled. The total site occupancy on the M2 site was constrained to unity, whereas on the M1 (Li) site, substoichiometry was allowed. The small fractions of site disorder atoms were fitted using fixed isotropic displacement factors, whereas the regular atoms, Li on M1 and Fe on M2 used anisotropic displacement factors. All other atoms were fitted with isotropic temperature factors. The atomic displacement of ions residing on the same site were coupled during the fit.

To restrict correlation effects, the anisotropic Li temperature factors were fixed to those resulting from fitting pristine micron sized $LiFePO_4$ material,[10] consistent with leading to displacement ellipsoids elongated towards the theoretical curved one-dimensional lithium diffusion path.[26] This is a reasonable assumption, given that the dopant leads to only very small distortions of the $LiFePO_4$ structure.

Combined X-ray and neutron diffraction refinements were performed using the GSAS program[27] with the EXPGUI interface.[28] The background of the neutron data was fitted with 9 terms (function type 4 in GSAS), and the X-ray data were fit with 7 terms (function type 1 in GSAS). Both the neutron and the X-ray diffraction line shape were fitted using function type 4 in GSAS. This accounts for anisotropic strain broadening described by a semi-empirical form[29] for orthorhombic $LiFePO_4$ using the Laue class *mmm*. Additionally, the isotropic particle size broadening was refined. Discrimination of the size and strain broadening was possible due to the large *d*-spacing range provided by the TOF neutron diffraction data. All refinements resulted in residuals R_{wp} and R_{exp} less than 3%, which indicates an excellent fit. All atomic positions, occupancies, cell parameters and phase fractions reported were based on the refinements as described above. The statistical errors quoted in the Tables of refined data are those conventionally obtained from the refinements, although we allow that these may be unrealistically low for site occupancies and thermal parameters owing to the difficult in independently refining these parameters.

Refinement of both anisotropic size and strain broadening parameters is very challenging even though TOF neutron diffraction data provides a large *d*-spacing range. The TEM images in Fig. 1 show particle elongation in the *c*-direction, indicating that isotropic size broadening can not be assumed. The size broadening is preferentially in the *ab*-plane, as observed by TEM, whereas the strain broadening is preferentially in the *bc*-plane. In this instance, the Fullprof program[30,31] was used to make a reasonable distinction. The background was refined by adjusting the height of preselected points for linear interpolation, and for the diffraction profile the pseudo-Voigt function[32] was used. Spherical harmonics[33] were used to model the anisotropic size broadening from which the average apparent crystallite size along the three reciprocal lattice vectors was calculated. The average crystal shape can be visualized by using the GFOURIER program.[34] For accurate description of the shape of the Bragg reflections the anisotropic strain-broadening model corresponding to the Laue class *mmm* was used. This leads to the average maximum strain of which the standard deviation is a measure of the degree of anisotropy.[35]

Results and discussion

I. Synthesis of nanocrystalline $LiFePO_4$

The $LiFePO_4$ samples were prepared under various reaction times (3–20 h) to study the effect on crystallite size. During the

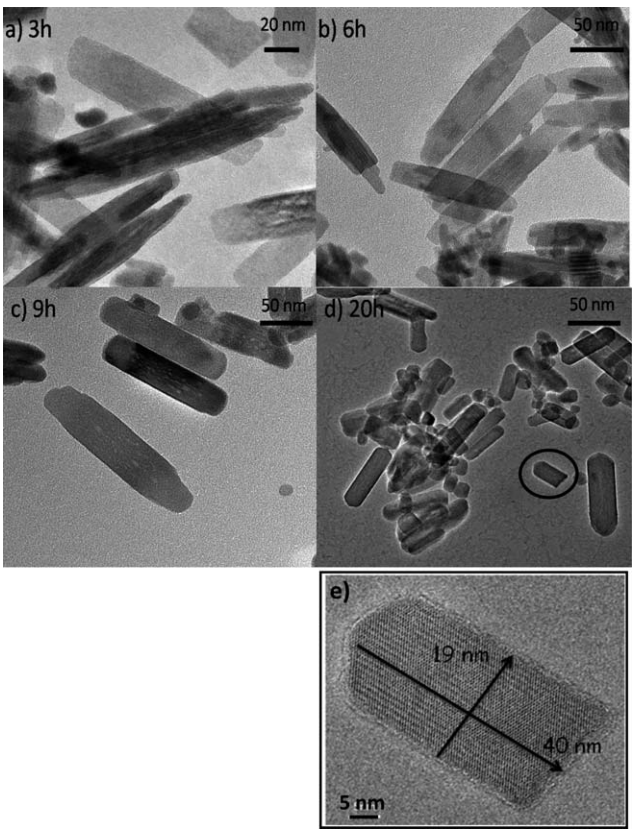

Fig. 1 TEM images of $LiFePO_4$ after reflux for (a) 3 h, (b) 6 h, (c) 9 h and (d) 20 h. A closeup of a single particle after 20 h of reflux is shown in (e), depicting it is a single crystallite.

synthesis, the polyol medium acts as both a solvent and a stabilizer, limiting particle growth and prohibiting agglomeration. It also circumvents any complications seen with aqueous preparation methods,[24] where protons may be incorporated into the lattice. The average crystallite coherence length, *d*, was calculated from the line width of the XRD patterns (supplemental information) using the Scherrer formula, as summarized in Table 1. Almost all the diffraction peaks broadened when the reaction time was reduced, indicating an isotropic decrease in the coherence length. As the tunnels occupied by Li in the structure are parallel to the *b*-axis, reduction of the particle size along the [010] direction is particularly significant to improve the accessibility of active material to the electrolyte, and reduce the Li^+ diffusion distance. The crystallite size along the [00l] direction could not be calculated due to the weak intensity of those reflections. The coherence lengths suggest that crystallite sizes are very small (15–20 nm) along the *a* and *b* directions. This was confirmed by TEM images (Fig. 1), which show the presence of anisotropic crystallites. Samples refluxed for 3 h produced 15 × 50 nm nano-needles which nucleate and grow into ~25 × 100 nm sized nano-rods with an increased reaction time of 20 h. The coherence lengths along [010] and [001] directions of the samples prepared by 3 and 20 h crystallization are in accord with the shortest crystal dimensions observed for these samples from the TEM studies, as shown in Fig. 1e. The long axis of the crystals was determined to be the c-axis by selected area electron diffraction (SAED). These studies suggest that nanocrystallites obtained from these samples are single crystallites and also that anisotropic growth takes place in the [001] direction.

Results of the simultaneous X-ray and neutron refinement on $LiFePO_4$ protected from air exposure are summarized in Table 1 and the neutron diffraction pattern is shown in Fig. 2. Fitting of the $LiFePO_4$ material prepared by 20 h of refluxing led to the exact site occupancies predicted by stoichiometry, with a unit cell volume of 290.66(1) Å^3. Although the Li on the M1 site occupancy refines to 1.0, we note that cell volumes for $LiFePO_4$ vary considerably depending on synthesis methods, with the high cell volumes (>291.5 Å^3) associated with low temperature methods that give rise to a high degree of anti-site mixing; and low cell volumes (<291.5 Å^3) characteristic of nanocrystallites prepared by precipitation or polyol methods.

The valence state of Fe in the prepared olivines was probed using Mössbauer spectroscopy and the results are shown in Fig. 3. The materials were exposed to air during the measurement and as a result, surface oxidation occurred as shown previously for nanoparticles of $LiFePO_4$.[23] These surface reactions include spontaneous lithium extraction from the bulk crystal and oxidative contamination on the particle surface and have been shown to have fast kinetics for nanoparticles of $LiFePO_4$.[36] As a result, the Fe^{+3} content in our $LiFePO_4$ was 6% and the spectrum is nearly identical to that of a sample of 40 nm crystallites exposed to air for one day from a previous report.[23] The broad profile of the Fe^{+3} component indicated that the Fe^{+3} ions were not dispersed throughout the lattice and thus oxidation was limited to the surface of the particles.

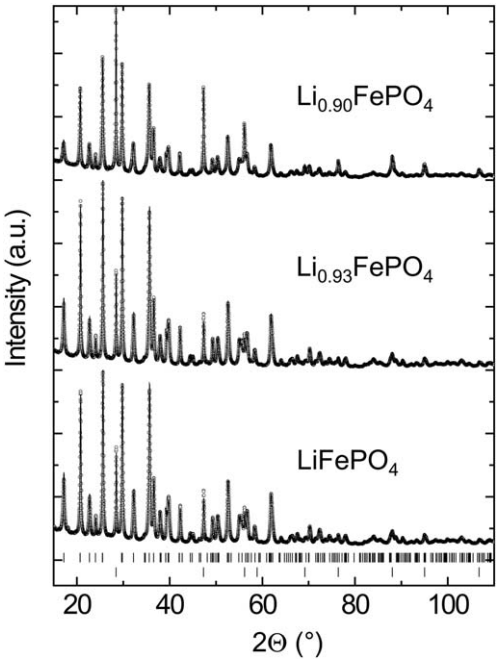

Fig. 2 Refined data for X-ray diffraction patterns of $LiFePO_4$, $Li_{0.93}FePO_4$ and $Li_{0.90}FePO_4$.

II. Direct synthesis of the substoichiometric series $Li_{1-x}FePO_4$

Sub-stoichiometric $LiFePO_4$ was synthesized directly, by modifying the quantity of the starting reagents in the polyol reaction. Two compositions were targeted: $Li_{0.9}FePO_4$ and $Li_{0.8}FePO_4$. Preliminary XRD studies showed both compounds to be pure olivine phases with some reflection intensity differences compared with $LiFePO_4$, however no impurity phases or amorphous components were detected. This is in contrast to previous attempts to make sub-stoichiometric olivine by a high-temperature solid-state route, where $Fe_2P_2O_7$ was found to be a common impurity.[8,37] Results of the combined X-ray and neutron refinements on the sub-stoichiometric olivines protected from air exposure are summarized in Table 1 and neutron diffraction patterns are shown in Fig. 2. The stoichiometries targeted were not the same as those obtained, as summarized in Fig. 4a: the target composition of $Li_{0.9}FePO_4$ refined to $[Li_{0.93}Fe_{0.01}][Li_{0.01}Fe_{0.99}]PO_4$ and the $Li_{0.8}FePO_4$ target composition refined to $[Li_{0.90}Fe_{0.03}][Li_{0.03}Fe_{0.97}]PO_4$, herein referred to by their M1 Li stoichiometry (ie. $Li_{0.93}FePO_4$ and $Li_{0.90}FePO_4$ respectively). In

Table 1 Refined unit cell and atomic parameters and atom parameters for directly synthesized $LiFePO_4$, $Li_{0.93}FePO_4$ and $Li_{0.90}FePO_4$

Composition	*a*/Å	*b*/Å	*c*/Å	*V*/Å^3	LiM1	FeM1	FeM2	LiM2
$LiFePO_4$	10.3217(3)	5.9987(1)	4.6943(1)	290.66(1)	1.000(7)	0.000(2)	1.000(1)	0.000(2)
$Li_{0.93}FePO_4$	10.3195(3)	5.9971(2)	4.6955(1)	290.59(1)	0.931(9)	0.012(1)	0.988(1)	0.012(2)
$Li_{0.90}FePO_4$	10.3306(3)	6.0024(1)	4.6983(1)	291.33(1)	0.898(8)	0.029(1)	0.971(1)	0.029(2)

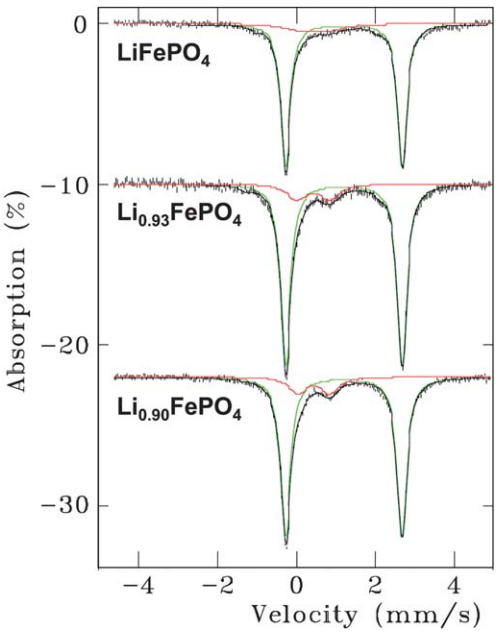

Fig. 3 Mössbauer spectra and fits for $LiFePO_4$, $Li_{0.93}FePO_4$ and $Li_{0.90}FePO_4$.

$Li_{0.93}FePO_4$, M1 vacancies are created by the lower lithium content, which also leads to anti-site mixing: 1.2% of the Fe ions reside on the M1 site, and conversely 1.2% of the Li ions reside on the M2 site, thus the more thermodynamically-stable olivine M2 site remains fully occupied. The existence of anti-site mixing along with site vacancies subtly influences the cell volume of the resultant olivine. The Shannon radius of Fe^{+2} (78 pm) is larger than that of Li^+ (76 pm) and Fe^{+3} (65 pm),[38] thus the implied presence of Fe^{3+} in the two aforementioned stoichiometries would reduce the unit cell volume. In contrast, the anionic repulsion at M1 site vacancies causes local expansion of the M1 site, as does the substitution of the larger Fe^{+2} ion for Li^+ on the M1 site. The effect of Li substoichiometry and anti-site defects on unit cell volume are summarized in Fig. 4b. With 6% M1 vacancies and a low degree (1.2%) of anti-site mixing, the net effect of the counteracting phenomena is minimal: the refined unit cell parameters and cell volume of $Li_{0.93}FePO_4$ were nearly identical to that of stoichiometric $LiFePO_4$ (see Table 1). With slightly more M1 vacancies (and hence more Fe^{+3} in the lattice) but a much larger degree of anti-site mixing (3.2% Fe on the M1 site), the refined unit cell volume of $Li_{0.90}FePO_4$ was found to be noticeably larger than that for $LiFePO_4$. Since this compound, with 7% M1 vacancies, was produced when a stoichiometry of 20% Li vacancies was targeted, we conclude that 7% is the limit of vacancies sustainable in directly synthesized triphylite materials produced by the polyol method and within the reported lithium deficient limit in $Li_{1-x}FePO_4$.[23] Targeting compounds of further Li sub-stoichiometry resulted in the formation of impurity phases, notably the sarcopside $Fe_3(PO_4)_2$ phase.

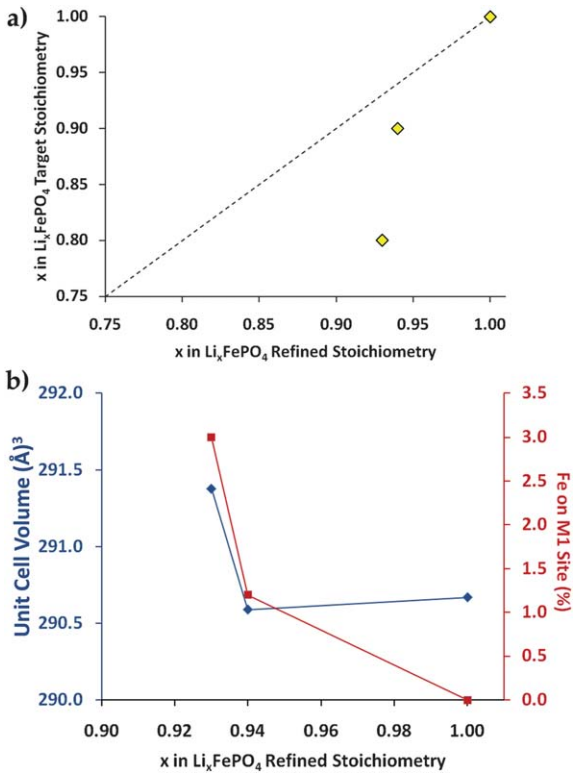

Fig. 4 (a) Plot of refined Li stoichiometry *vs.* target stoichiometry for Li_xFePO_4; (b) Plot of anti-site defect concentration and unit cell volume with respect to refined substoichiometry for Li_xFePO_4.

Mössbauer analysis of these directly-synthesized sub-stoichiometric olivines (Fig. 3) verified the quantity of Fe^{3+} indirectly determined by the refinement of the vacancy concentration from the diffraction data. In addition to the Fe^{2+} signal, a Fe^{3+} signal is present in both the $Li_{0.93}FePO_4$ and $Li_{0.90}FePO_4$ samples, whose intensity increases with the degree of substoichiometry: this feature comprised 14% and 16% of the spectrum respectively for $Li_{0.93}FePO_4$ and $Li_{0.90}FePO_4$. As a result of surface oxidation caused by air exposure, the quantity of Fe^{3+} in these samples is higher than the stoichiometry predicted. Since all samples possessing similar crystallite size were handled in an identical manner, a 6–8% Fe^{3+}-surface contribution was subtracted. We conclude that both substoichiometric samples are similar in lattice Fe^{3+} content, namely about 6–7%, in accord with our neutron and XRD diffraction studies.

III. Study of the delithiated samples

To study the effect of anti-site disorder on delithiation, $Li_{1.0}FePO_4$, $Li_{0.93}FePO_4$ and $Li_{0.90}FePO_4$, which possess increasing fractions of anti-site disorder of 0.0%, 1.2% and 2.9% respectively, were chemically delithiated to $Li_{0.5}FePO_4$ using $NOBF_4$. Combined XRD and ND studies were performed on these compositions and the cell parameters and site occupancies obtained from the delithiation study are summarized in Table 2. As expected, partial delithiation of the olivines produces a two-phase mixture of a lithium-rich and a lithium-poor stiochiometry. On delithiation of stoichiometric $LiFePO_4$, the cell volume of the Li-rich end member decreases slightly from the volume of the starting composition, indicative of the formation of a solid solution whose composition was determined to be $Li_{0.90}FePO_4$. The degree of Li vacancies sustained in this partially oxidized phase (about 10%) is similar to other such phases formed in nanoparticulate $LiFePO_4$ by electrochemical oxidation[23,39] and

Table 2 Unit cell parameters and atom parameters from simultaneous refinement of the X-ray and neutron data for $Li_{1.0}FePO_4$ and $Li_{0.93}FePO_4$, each delithiated to $Li_{0.5}FePO_4$. Phase α and β refer to the Li-poor and Li-rich phase respectively

Li_xFePO_4	Phase	*a*/Å	*b*/Å	*c*/Å	*V*/Å^3	Fe	Li	FeM1
$x = 1$	α	9.8294(3)	5.7998(1)	4.7843(1)	272.75(1)	0.999(1)	0.108(15)	0.002(2)
	β	10.2859(3)	5.9771(1)	4.7119(1)	289.69(1)	1.002(2)	0.903(17)	0.001(1)
$x = 0.93$	α	9.8297(3)	5.7994(1)	4.7848(1)	272.77(1)	1.001(1)	0.097(13)	0.001(1)
	β	10.3189(3)	5.9983(1)	4.6988(1)	290.84(1)	0.978(1)	0.904(14)	0.022(1)

by exposure to air.[23] In each of these cases, the partial delithiation is accompanied by a small reduction (<2%) in the unit cell volume and we observe a decrease in unit cell volume of 0.34%. The extended solid solution supports reduction in the miscibility gap with reduced size of insertion materials as proposed previously[22,23,39] and recently predicted by Wagemaker *et al.*[40] and Burch *et al.*,[41] the latter based on the diffuse interface introduced by Cahn and Hilliard.[42]

In contrast, $Li_{0.93}FePO_4$ undergoes a subtle unit cell expansion upon delithiation to $Li_{0.50}FePO_4$. This is a direct result of the delithiation of defect-free portions of the crystallites: the Li-poor phase was found to be free of defects. The concentration of defects in the Li-rich region approximately doubles (to 2.2%) since the number of defects remains unchanged while the quantity of the Li-rich region has been reduced by roughly half. The increase in unit cell volume expected by the higher defect concentration offsets the decrease in unit cell volume anticipated by the lower Li stoichiometry in the Li-rich phase which was determined to be $Li_{0.90}FePO_4$, the same as in the aforementioned case of delithiated $LiFePO_4$.

We prepared a large series of compounds by the chemical oxidation of the sample with the highest anti-site defect concentration, $Li_{0.90}FePO_4$. The data from the Rietveld refinements are summarized in Table 3 and a schematic diagram is shown in Fig. 5. Refinement of the material formed on partial delithiation to $Li_{0.60}FePO_4$ revealed the expected formation of a Li-rich and a Li-poor phase, each of which have an extended solid solution composition. The Li-poor phase was found to be free of anti-site defects, indicating preferential delithiation of defect-free regions. Of particular interest was the composition of the Li-poor phase, determined to be $Li_{0.14}FePO_4$ after a combined X-ray and neutron refinement. This lithium content is higher than any reported for any Li-poor triphylite phase formed by electrochemical methods.[22,23,39] The unit cell volume of this phase, 273.82(1) Å^3, is substantially larger than typical values of bulk $FePO_4$ (271.7–272.4 Å^3)[2,22,43] and close to that reported for Li-poor phases in nanoparticulate $LiFePO_4$ electrochemically delithiated to a 50% state of charge (274.3 Å^3) although the stoichiometry of the Li-poor phase was not accurately determined in that case.[39] The Li-rich phase in the $Li_{0.90}FePO_4$ delithiated to $Li_{0.60}FePO_4$ exhibits minimal change in composition: stoichiometry remains $Li_{0.93}FePO_4$ (within error), the anti-site defect concentration remains at 3% and the unit cell volume experiences minimal contraction.

Further delithiation to $Li_{0.5}FePO_4$ revealed that Li removed at this step was extracted from both the Li-poor phase, which undergoes a notable decrease in Li content (down to $Li_{0.11}FePO_4$) and a unit cell contraction of 0.37%, and the Li-rich phase. The Li-poor phase remains free of anti-site defects, further verifying the preferential delithiation of defect-free regions of the crystallites.

Delithiation to $Li_{0.3}FePO_4$ showed a more obvious decrease in the Li stoichiometry of the Li-rich phase, to $Li_{0.87}FePO_4$. The unit cell volume decreased accordingly, to 290.92(1) Å^3. The stoichiometry of the Li-poor phase remained the same ($Li_{0.11}FePO_4$) as the previous step, but at this stage, there were no more pristine regions of the crystallites to delithiate. At this point, the defect-containing regions of the crystallite started to delithiate, as evidenced by the presence of Fe on the M1 site in the Li-poor phase. The unit cell volume of the Li-poor phase also experienced a slight increase, as expected. An important conclusion of the evolution of the anti site disorder fractions in two phases upon delithiation, summarized in Fig. 5, is that the anti-site disorder defects are aggregated. This supports previous discussions of the defect chemistry and possible association (trapping) in $LiFePO_4$,[44] that called for atomistic modeling to quantify the energies of association. In fact, such recent studies predict significant negative binding energies (>−0.6 eV) for neutral one-dimensional clusters along the *b*-axis channel comprised of anti-site defects ($Fe^{\bullet}_{Li}$) and Li vacancies.[18,45] The binding energies suggest the clustering of defects is important as a precursor to local ordering or nanodomain formation, which is what we observe here (*vide infra*).

Table 3 Unit cell parameters and atom parameters from simultaneous refinement of the X-ray and neutron data for $Li_{0.90}FePO_4$ delithiated to various compositions. Phase α and β refer to the Li-poor and Li-rich phase respectively

Li_xFePO_4	Phase	*a*/Å	*b*/Å	*c*/Å	*V*/Å^3	LiM1	FeM1	FeM2	LiM2
$x = 0.90$	β	10.3306(3)	6.0024(1)	4.6983(1)	291.33(1)	0.898(8)	0.029(1)	0.971(1)	0.029(2)
$x = 0.6$	α	9.8529(3)	5.8078(1)	4.7851(1)	273.82(1)	0.136(22)	0.000(2)	1.001(2)	0.000(2)
	β	10.3288(3)	5.9989(1)	4.7010(1)	291.28(1)	0.933(8)	0.029(1)	0.971(1)	0.029(1)
$x = 0.5$	α	9.8317(3)	5.7990(1)	4.7856(1)	272.83(1)	0.113(23)	0.002(2)	1.002(2)	0.002(2)
	β	10.3211(3)	5.9992(1)	4.7009(1)	291.07(1)	0.917(13)	0.048(1)	0.952(1)	0.048(1)
$x = 0.3$	α	9.8425(2)	5.8012(1)	4.7850(1)	273.22(1)	0.110(9)	0.011(1)	0.989(1)	0.011(1)
	β	10.3079(3)	5.9910(1)	4.7109(1)	290.92(1)	0.865(17)	0.038(2)	0.962(2)	0.038(2)
$x = 0$	α	9.8276(2)	5.7998(1)	4.7797(1)	272.43(1)	0.019(2)	0.032(1)	0.968(2)	0.032(1)

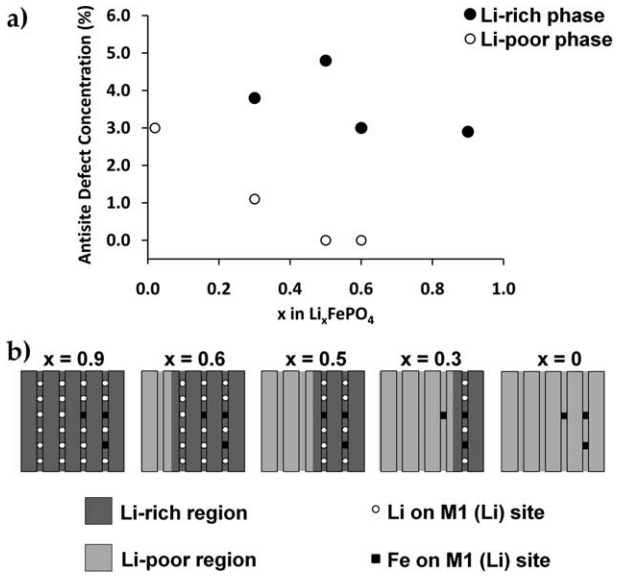

Fig. 5 Interpretation of fit results for delithiation of $Li_{0.90}FePO_4$: composition dependence and site disorder. (a) Plot showing evolution of site defects in the Li-rich and Li-poor phases as a function of delithiation; (b) overall schematic that shows evolution of phase segregation of the Li-rich and Li-poor regions of the crystallites with regions free of Fe anti-site defects delithiating before regions containing M1 site defects.

Despite the presence of 3% Fe on the M1 site in the as-prepared $Li_{0.90}FePO_4$ sample, almost complete delithiation of this sample could be achieved. The content of Fe on the M2 site is approximately 0.97, thus we assume the remaining 3% of those sites to still contain Li, owing to the implication that the M2 site must always be fully occupied owing to the higher thermodynamic stability of the M2 site with respect to the M1 site. The Li situated on the M2 site did not diffuse into the M1 sites, even thought the M2 and M1 sites are edge-sharing, as are the M1–M1 sites in olivines. Even though certain Li channels are blocked with defects, all the Li on the M1 site were removed by chemical delithiation from the lattice; it is implied that Li ions trapped in tunnels parallel to the *b*-axis containing multiple defects are able to be extracted from the lattice *via* higher activation energy pathways along the *a*-axis or *c*-axis.[14,15]

The diffraction patterns provide two clear indications of coexistence of the Li-rich and Li-poor phases within one coherent crystallite. As such, anisotropic strain broadening preferential in the *bc*-plane was required for accurate fits, consistent with the phase boundary in the *bc*-plane as experimentally observed in microparticles by Richardson *et al.*,[46] minimizing the strain that is the result of the lattice mismatch.[40] This result is a clear signature of phase a coherent interface between the two coexisting phases: upon delithiation substantial size broadening of the peaks in the corresponding Li-rich phases of delithiated compounds was observed (see Supplemental info). We note that the existence of a coherent interface may well depend on the particle size: its absence has been observed in $LiFePO_4$[47] and other insertion materials such as TiO_2,[51] where nanocrystallites were found to have either the lithium poor or lithium rich phase. The fact that the phases coexist in the nanoparticles studied here is therefore an important result.

The large *d*-spacing range probed by TOF diffraction allowed differentiation of the anisotropic broadening due to strain from that originating from particle shape, the latter clearly observed in the TEM in Fig. 1. The average domain size as calculated from anisotropic size broadening increases as the Li-poor regime grows upon delithiation, which mirrors a decrease in the domain size in the Li-rich regime. The evolution in domain size and phase fractions of the two phases obtained from analysis of the refined data is summarized in Fig. 6. The increase in the phase fraction of the Li-poor fraction correlates exactly to the decrease in the Li-rich phase. Continuous increase in the domain size of $FePO_4$ phase at the expense of the $LiFePO_4$ domain size with increased delithiation, while the sum of domain sizes being nearly equal to the domain size of pure $LiFePO_4$ or pure $FePO_4$, suggests the presence of a single domain for each phase in a crystallite as opposed to multiple grain boundaries as observed in large hydrothermally prepared crystals.[46] The suggests phase coexistence within the same particle supports the delithiation model put forward by Laffont *et al.*[48] rather than a mixture of monophasic particles as reported previously.[47] These Li-rich and Li-poor domains of smaller size (20–30 nm) exhibit an extended solid solution which suggests that synthesis of nano-$LiFePO_4$ with smaller crystallite size (20–25 nm) would result in the extended solid solution in two end phases over the entire crystallite.

IV. Electrochemistry

The role of M1/M2 site disorder is especially prevalent in the electrochemical data for these compounds. The charge-discharge

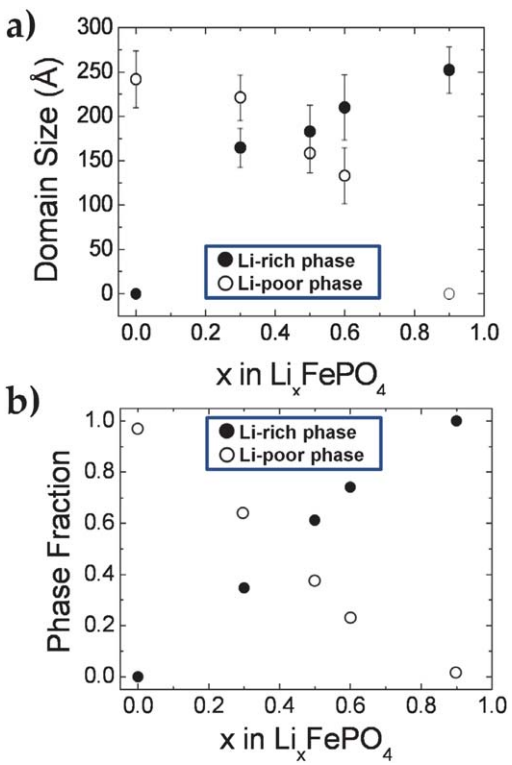

Fig. 6 (a) Domain size from reflection broadening and (b) phase fractions as a function of delithiation of $Li_{0.90}FePO_4$. The open circles refer to the Li-poor phase, and the closed circles to the Li-rich phase, as in Fig. 5.

profiles for $LiFePO_4$ and $Li_{0.90}FePO_4$, cycled at a rate of C/10 *vs.* Li/Li^+ are shown in Fig. 7. At this rate, cells containing nano-particluate $LiFePO_4$ can be fully charged then discharged to 93% of the theoretical capacity (170 mAh/g). The polarization between the charge and discharge curves is very low (50 mV). In pure ordered $LiFePO_4$, delithiation occurs as predicted by theoretical calculations along the (010) direction and Li-ions are not required to cross between Li channels through high energy barriers. The electrochemical profile of the substoichiometric $Li_{0.90}FePO_4$ material with 2.9% anti-site mixing differs from that of $LiFePO_4$. Charging the cell results in deintercalation of only 0.65 Li, which implied a portion of the electrochemical capacity was irreversibly trapped in the anti-site defect-rich regions. In discharge, the cell reintercalates 0.72 Li, corresponding to the complete reduction of the Fe^{3+} from both the electrochemical oxidation and the 7% Fe^{3+} present in the olivine phase after synthesis. The polarization in this sample was 80 mV, which is higher than the polarization for the ordered nano-$LiFePO_4$. An increase of polarization indicates kinetic hindrance and suggests blockage of the Li tunnels by the anti-site defects, which impede Li-ion movement and forces the adoption of higher-energy diffusion pathways.[18,49] Similar behavior and reduced capacity has been reported recently for $LiFePO_4$ samples doped with 5% of Mg/Zr in the M1 site[13] and for another defect-laden olivine, $Li_{0.79}FePO_4$.[24] The latter exhibits a more pronounced sloping voltage charge/discharge curve although the origin of this effect, whether a result of a higher degree of anti-site mixing, or the aqueous solution preparation method that might introduce additional defects such as H^+ in the lattice, is not clear.

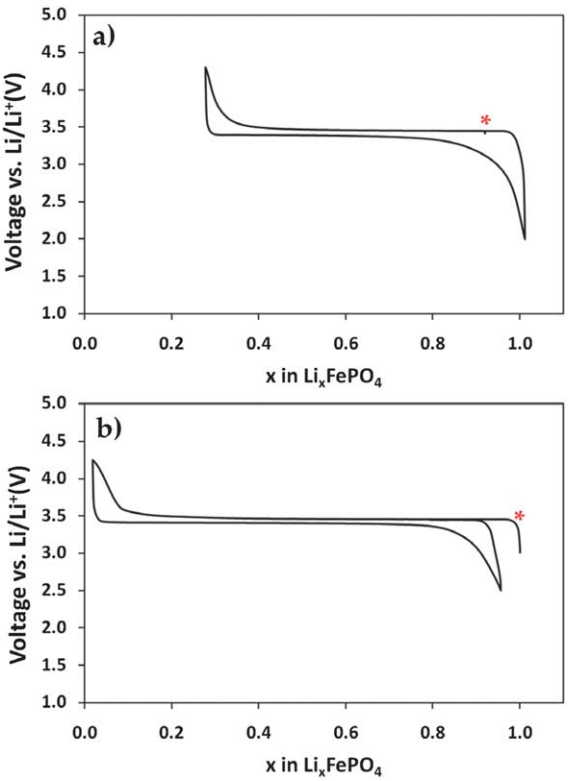

Fig. 7 Electrochemical data for observed stoichiometries $LiFePO_4$ and $Li_{0.90}FePO4$ both made by the polyol method: red asterisk indicates starting stoichiometry.

Conclusions

The present results show that careful particle size control may be achieved in the synthesis of $LiFePO_4$ from a modified polyol method. $LiFePO_4$ may be prepared in this manner to be free of anti-site defects which allows for almost full electrochemical reversibility which is unusual with olivines prepared at temperatures lower than 350 °C. The nanoparticles produced from this synthesis are able to sustain isolated regions of solid solution of approximately 10% Li vacancies in the Li-rich phase and 10% Li content in the Li-poor phase.

In an attempt to introduce high ionic mobility, lithium-deficient solid solutions were directly synthesized, resulting in a significant substoichiometry where up to 7% vacancies on the M1 (Li) site could be sustained as determined by combined neutron and X-diffraction studies, and confirmed by Mössbauer spectroscopy. Reduction of Li in the target stoichiometry led to the formation of considerable concentrations of anti-site defects which tend to cluster owing to their electrostatic and elastic interactions, as illustrated by the preferential delithiation of defect-free regions over a substantial Li-domain. This causes phase segregation of defect-rich and defect-free regimes. Our findings offer definitive experimental proof, and confirm theoretical calculations that predict negative binding energies between anti-site defects and hence promote the formation of defect clusters.[18] This affects Li-ion conductivity, as proposed elsewhere,[45] owing to entrapment of the migrating Li^+ vacancies. Defect clustering therefore inhibits Li extraction, because the defect cluster regions are more likely to retain lithium. Although thermodynamically unfavorable,[40] anisotropic strain broadening and domain size broadening upon delithiation also show that the Li-poor and Li-rich phases coexist within one nano-particle, unlike what is observed in other nano-sized insertion compounds.[50,51] Theoretically, an ideal $LiFePO_4$ electrode material would be comprised of perfectly ordered nano (<30 nm) $LiFePO_4$, exhibiting a complete solid solution over the entire Li-domain. Smaller particles would also have the advantage of smaller diffusion distance. Our polyol method allows for the synthesis of nanoparticles without the formation of lattice defects which is difficult to avoid with typical low temperature synthetic methods usually necessary to obtain nanoparticles.

Acknowledgements

LFN gratefully acknowledges NSERC through funding from its Discovery, Canada Research Chair and Collaborative Research Grant (with GM) programs. The authors thank Ron Smith for assistance with the neutron diffraction experiments at POLARIS (ISIS) and Dr Gianluigi Botton at McMaster University for providing TEM images. The Netherlands Organization for Scientific Research NWO is acknowledged for the CW-VIDI grant of M.W.

References

1 A. K. Pahdi, K. S. Nanjundaswamy, C. Masquelier, S. Okada and J. B. Goodenough, *J. Electrochem. Soc.*, 1997, **144**, 1609.
2 A. K. Pahdi, K. S. Nanjundaswamy and J. B. Goodenough, *J. Electrochem. Soc.*, 1997, **144**, 1188.
3 H. Huang, S. C. Yin and L. F. Nazar, *Electrochem. Solid-State Lett.*, 2001, **4**, A170.

4 M. Gaberscek, R. Dominko and J. Jamnik, *Electrochem. Commun.*, 2007, **9**, 2778.
5 M. Maccario, L. Croguennec, B. Desbat, M. Couzi, F. Le Cras and L. Servant, *J. Electrochem. Soc.*, 2008, **155**, A879–A886.
6 Y. Wang, Y. Wang, E. Hosono, K. Wang and H. Zhou, *Angew. Chem., Int. Ed.*, 2008, **47**, 1–6.
7 B. Kang and G. Ceder, *Nature*, 2009, **458**, 190–193.
8 P. S. Herle, B. Ellis, N. Coombs and L. F. Nazar, *Nat. Mater.*, 2004, **3**, 147–152.
9 Y.-M. Chiang, S.-Y. Chung, J. T. Bloking, A. M. Andersson, Patent US 7,338,734 B2, 2008.
10 M. Wagemaker, B. L. Ellis, D. Luetzenkirchen-Hecht, F. M. Mulder and L. F. Nazar, *Chem. Mater.*, 2008, **20**, 6313–6315.
11 A. Goni, L. Lezama, M. I. Arriortua, G. E. Barberisa and T. Rojo, *J. Mater. Chem.*, 2000, **10**, 423–428.
12 A. Goni, L. Lezama, A. Pujana, M. I. Arriortua and T. Rojo, *Int. J. Inorg. Mater.*, 2001, **3**, 937–942.
13 N. Meethong, Y.-H. Kao, S. A. Speakman and Y.-M. Chiang, *Adv. Funct. Mat*, 2009, **19**, 1–11.
14 D. Morgan, A. Van der Ven and G. Ceder, *Electrochem. Solid-State Lett.*, 2004, **7**, A30–A32.
15 M. S. Islam, D. J. Driscoll, C. A. J. Fisher and P. R. Slater, *Chem. Mater.*, 2005, **17**, 5085–5092.
16 R. Amin, P. Balaya and J. Maier, *Electrochem. Solid-State Lett.*, 2007, **10**, A13–A16.
17 J. Li, W. Yao, S. Martin and D. Vaknin, *Solid State Ionics*, 2008, **179**, 2016–2019.
18 C. A. J. Fisher, V. M. H. Prieto and M. S. Islam, *Chem. Mater.*, 2008, **20**, 5907–5915.
19 S. F. Yang, P. Y. Zavalij and M. S. Whittingham, *Electrochem. Commun.*, 2001, **3**, 505–508.
20 J. J. Chen and M. S. Whittingham, *Electrochem. Commun.*, 2006, **8**, 855–858.
21 S.-Y. Chung, S.-Y. Choi, T. Yamamoto and Y. Ikuhara, *Phys. Rev. Lett.*, 2008, **100**, 125502-1–125502-4.
22 A. Yamada, H. Koizumi, S. I. Nishimura, N. Sonoyama, R. Kanno, M. Yonemura, T. Nakamura and Y. Kobayashi, *Nat. Mater.*, 2006, **5**, 357–360.
23 G. Kobayashi, S. Nishimura, M. S. Park, R. Kanno, M. Yashima, T. Ida and A. Yamada, *Adv. Funct. Mater.*, 2009, **19**, 395–403.
24 P. Gibot, M. Casas-Cabanas, L. Laffont, S. Levasseur, P. Carlach, S. Hamelet, J. M. Tarascon and C. Masquelier, *Nat. Mater.*, 2008, **7**, 741–747.
25 D.-H. Kim and J. Kim, *Electrochem. Solid-State Lett.*, 2006, **9**, A439–A442.
26 S. Nishimura, G. Kobayashi, K. Ohoyama, R. Kanno, M. Yashima and A. Yamada, *Nat. Mater.*, 2008, **7**, 707–711.
27 A. C. Larson, R. B. Von Dreele, *Los Alamos National Laboratory Report LAUR 86-748*, 2000.
28 B. H. Toby, *J. Appl. Crystallogr.*, 2001, **34**, 210.
29 P. W. Stephens, *J. Appl. Crystallogr.*, 1999, **32**, 281–289.
30 J. Rodriguez-Carvajal, *Phys. B*, 1993, **192**, 55–69.
31 J. Rodriguez-Carvajal, Recent Developments of the Program FULLPROF, in *CPD Newsletter*2001, 26, 12, available at http://www.ill.eu/sites/fullprof/index.html.
32 P. Thompson, D. E. Cox and J. B. Hastings, *J. Appl. Crystallogr.*, 1987, **20**, 79–83.
33 M. Jarvinen, *J. Appl. Crystallogr.*, 1993, **26**, 525–531.
34 J. Gonzales-Platas; J. Rodriguez-Carvajal, *Graphic Fourier Program GFOURIER*, Version 04.02. Univ. La Laguna, Tenerife, Spain, 2002.
35 J. Rodriguez-Carvajal, M. T. Fernandez-Diaz and J. Martinez, *J. Phys.: Condens. Matter*, 1991, **3**, 3215–3234.
36 J. F. Martin, A. Yamada, G. Kobayashi, S. Nishimura, R. Kanno, D. Guyomard and N. Dupre, *Electrochem. Solid-State Lett.*, 2008, **11**, A12–A16.
37 B. Ellis, P. S. Herle, Y. H. Rho, L. F. Nazar, R. Dunlap, L. K. Perry and D. H. Ryan, *Faraday Discuss.*, 2007, **134**, 119–141.
38 R. D. Shannon, *Acta Crystallogr. A*, 1976, **A32**, 751–767.
39 N. Meethong, H.-Y. S. Huang, W. C. Carter and Y.-M. Chiang, *Electrochem. Solid-State Lett.*, 2007, **10**, A134–A138.
40 A. Van der Ven, K. Garikipati, S. Kim and M. Wagemaker, *J. Electrochem. Soc.*, 2009, **156**, A949–A957.
41 D. Burch and M. Z. Baant, *Nano Lett.*, 2009, **9**, 3795–3800.
42 J. W. Cahn and J. E. Hilliard, *J. Chem. Phys.*, 1958, **28**, 258–267.
43 A. M. Andersson, B. Kalska, L. Haggstrom and J. O. Thomas, *Solid State Ionics*, 2000, **130**, 41–52.
44 J. Maier and R. Amin, *J. Electrochem. Soc.*, 2008, **155**, A339.
45 G. Gardiner and M. S. Islam, *Chem. Mater.*, 2010, **22**, 1242–1248.
46 G. Chen, X. Song and T. J. Richardson, *Electrochem. Solid-State Lett.*, 2006, **9**, A295–A298.
47 C. Delmas, M. Maccario, L. Corguennec, F. Le Cras and F. Weill, *Nat. Mater.*, 2008, **7**, 665–671.
48 L. Laffont, C. Delacourt, P. Gibot, M. Y. Wu, P. Kooyman, C. Masquelier and J. M. Tarascon, *Chem. Mater.*, 2006, **18**, 5520–5529.
49 R. Malik, D. Burch, M. Bazant, G. Ceder, *Nano Lett.*, in press.
50 H. G. Schimmel, J. Huot, L. C. Chapon, F. D. Tichelaar and F. M. Mulder, *J. Am. Chem. Soc.*, 2005, **127**, 14348–14354.
51 M. Wagemaker, W. J. H. Borghols and F. M. Mulder, *J. Am. Chem. Soc.*, 2007, **129**, 4323–4327.